Article

Tissue-Engineered Trachea Consisting of Electrospun Patterned sc-PLA/GO-g-IL Fibrous Membranes with Antibacterial Property and 3D-Printed Skeletons with Elasticity

Yuan Kang, Chaoli Wang, Youbei Qiao, Junwei Gu, Han Zhang, Ton Peijs, Jie Kong, Guangcheng Zhang, and Xuetao Shi

Biomacromolecules, **Just Accepted Manuscript** • DOI: 10.1021/acs.biomac.9b00160 • Publication Date (Web): 07 Mar 2019

Tissue-Engineered Trachea Consisting of Electrospun Patterned sc-PLA/GO-*g*-IL Fibrous Membranes with Antibacterial Property and 3D-Printed Skeletons with Elasticity

*Yuan Kang [a], Chaoli Wang [b], Youbei Qiao [b], Junwei Gu[a,d], Han Zhang[c,d], Ton Peijs[c,d], Jie Kong[a,d], Guangcheng Zhang [a] * and Xuetao Shi [a,d] **

[a] Department of Applied Chemistry, School of Natural and Applied Sciences, Northwestern Polytechnical University, Xi'an 710129, P. R. China

[b] Department of Pharmaceutical Analysis, School of Pharmacy, Fourth Military Medical University, Xi'an, 710032, China

[c] School of Engineering and Materials Science, Queen Mary University of London, Mile End Road, E1 4NS, London, UK

[d] NPU-QMUL Joint Research Institute of Advanced Materials and Structures, Northwestern Polytechnical University, Xi'an, 710072, PR China

KEYWORDS**:** tissue-engineered trachea; patterned electrospun fiber; 3D printing; antibacterial property; GO-*g*-IL

ABSTRACT:

In this study, tissue-engineered trachea, consisting of multilevel structural electrospun polylactide (PLA) membranes enveloping 3D-printed thermoplastic polyurethane (TPU) skeletons, was developed to create a mechanically robust, antibacterial and bioresorbable graft for the tracheal reconstruction. The study design incorporated two distinct uses of stereocomplex PLA: patterned electrospun fibers to enhance tissue integration compared to the random layered fibers, meanwhile possess good antibacterial property; and 3D-printed TPU scaffold with elasticity to provide external support and protection. Herein, ionic liquid (IL)-functioned graphene oxide (GO) was synthesized and presented enhanced mechanical and hydrophilicity properties. More interesting, antibacterial activity of the GO-*g*-IL modified PLA membranes were proved by *E. coli* and *S. aureus*, showing superior antibacterial effect compared to single GO or IL. The synergistic antibacterial effect could be related to that GO break cytomembrane of bacteria by its extremely sharp edges, while IL works by electrostatic interaction between its cationic structures and electronegative phosphate groups of bacteria membranes, leading to the loss of cell electrolyte and cell death. Hence, after L929 fibroblast cells were seeded on patterned fibrous membranes with phenotypic shape, further effectively cell infiltration, cell proliferation and attachment were observed. In addition, the tissue-engineered trachea scaffolds were implanted into rabbit models. The *in vivo* result confirmed that the scaffolds with patterned membranes manifested favorable biocompatibility and promoted tissue regeneration.

INTRODUCTION

The damage to the trachea or congenital tracheal stenosis of humans can result in great reduction in quality of life with problems of swallowing, speaking even breathing.[1] Tissue engineering provides scaffolds for tissue as temporal support for cells to regenerate new extracellular matrix (ECM), which tissue has been destroyed via congenital defects, disease, or injury.[2] Basic requirement of tissue-engineered trachea includes: suitable biomaterials, which should be biocompatible and vascularized to increase cellular adhesion; appropriate morphological structure and biomechanical properties; and an antibacterial surface to reduce the initial bacterial load.[3]

Polymer scaffolds manufactured by electrospinning method possess controllable 3D architectures of the fiber diameter from nanometer to micrometer range. Their high specific area makes such scaffolds enable to tissue engineering via promoting cell attachment and proliferation.[4-7] However, the electrospun scaffolds prepared by conventional method are made of disordered and very dense fibers. Although the opening porosity is very high, their pore sizes are smaller than the size of the cell, so it becomes a major factor limiting the penetration of the cell growth inside the fibrous scaffolds. In order to obtain scaffolds with suitable pore size promoting the cell infiltration, Visscher *et al*.[8] prepared polycaprolactone scaffolds with macro-microporosity by 3D printing technology, the induced macro-structure allowed the fibroblast cells to infiltrate inside the scaffolds. However, the rough framework of the scaffolds is not easily processed or used in miniature tissues. Mandal *et al*. [9] studied the effect of pore sizes of silk scaffolds manufactured by a salt leaching method. They found that when the pore sizes of scaffolds were larger than 60 μm, the structure of the scaffolds could promote tissue regeneration. The mechanical properties of scaffolds prepared by this method exhibited a tensile modulus below 1.4 MPa, which seems to be unable to meet the operating requirements. In literature, several strategies for surface texture and

patterning of fibers were reported. Peijs *et al* reported electrospun fibres by photoembossing method and studied the effect of surface texture on the cell adhesion.[10,11] Recently, Chen *et al.* applied direct writing electrospinning to prepare complex three-dimensional with macropore.[12] However, the relationship between structure of patterned fibrous scaffolds and cell infiltrating has not been systematically studied. In this study, we designed multileveled structural fibrous membranes by patterned electrospinning[13-16] for better cell infiltrating, the mechanical and hydrophilic properties of the fibrous membranes were also considered.

Furthermore, due to the direct contact of air inside the implanted trachea scaffold, large amounts of bacteria can pose a threat to the newly implanted trachea. Although there are many studies on the preparation and biocompatibility of artificial tracheas, most of these approaches concentrated only on regenerating tracheal epithelium and have not pay close attention to the endotracheal antibacterial capability.[3] Graphene oxide (GO) is a well-known monolayer of carbon atoms containing carboxylic, hydroxyl and epoxide groups on the surface of carbon layer structure[17,18]. Moreover, it has been reported as possessing powerful antimicrobial action by effective direct contact interaction with microorganisms using its extremely sharp edges, which may result in physical damages to cell membranes. Afterwards, the ensuing superoxide anion-independent oxidation could occur between GO and cell membranes to incapacitate the cells.[19-22] Therefore, GO serves as a platform for growing antibacterial particles or grafting antibacterial groups for a synergistic antibacterial effect.[23-25] Zhong *et al*.[26] loaded zinc oxide (ZnO) nanoparticles on GO nanosheets. These functioned GO sheets could destroy bacterial integrated membranes and prevent bacterial proliferation via Zn^{2+} and physical scratching by GO edges. Therefore, the concentration of bacteria cultured with ZnO/GO was significantly lower than with individual ZnO particles and GO nanosheets. Fathalipour *et al*.[27] also presented synergistic

nanocomposites by growing silver nanoparticles (AgNPs) on GO sheets. Compared with AgNPs, GO/Ag shows much higher antibacterial efficiency. In addition to metal nanoparticles, ionic liquids (ILs) are also recognized as having good antimicrobial effects.[28-30] Here, an electrostatic interaction will occur between cationic structures of the IL and electronegative phosphate groups of the microbial cell membranes. After that, the hydrophobic segments of IL inserts into the lipid cell membranes, leading to the loss of cell electrolyte and cell death.[31] However, there are very few reports of GO and ILs cooperating in antibacterial activity.

In literature, although several research groups have reported that patients with a clinically transplanted tissue-engineered trachea successfully regained anatomical structure and physiological function, there are still some obstacles that need to be addressed before this technique can be used routinely in the clinical setting[32]. One of the main issues with the use of tissue-engineered trachea is the complications that arise due to the immaturity of the transplanted graft. To achieve tissue maturation *in vitro* or *in vivo* prior to transplantation should be option. In vivo experiment involves the transplantation of the graft to another site of the body, or to immunodeficient mice and rats[33-35]. Park *et al.* developed a novel tissue-engineered trachea by three-dimensional (3D) printing of monolithic bellows, tracheal scaffolds was implanted into the dorsal subcutaneous spaces of each nude mouse[33]. Xu *et al.* investigated tissue-engineered trachea regeneration using decellularized rabbit trachea. The scaffolds were embedded subcutaneous[35].

In this study, combined trachea scaffolds were consisting of antibacterial patterned electrospun membranes with 3D-printed skeletons for promoting tissue regeneration. GO-g-IL was synthesized for charging the fibrous membranes synergetic antibacterial effect. Furthermore, patterned electrospun membranes of biodegradable PLA/ GO-g-IL was designed with multi-level structure to enhance the cell infiltration, together with positive effect on the mechanical and

hydrophilicity properties. The final tissue-engineered trachea was consisted of the electrospun pattered PLA/ GO-g-IL and 3D-printed skeletons with good elasticity to provide external support and protection. The mechanical, antibacterial properties and biocompatibility of patterned electrospun membranes and combined trachea scaffolds were investigated. The electrospun membranes and combined scaffolds were implanted into rabbit models for estimating the promotion of tissue growth.

EXPERIMENTAL SECTION

Materials. 3-chloropropyl-trimethoxy silane, vinyl imidazole and hexafluoroisopropanol were supplied from Sigma-Aldrich Inc, China. GO dispersion liquid was purchased from XFNANO Inc in Nanjing, China. poly (L-lactide) (PLLA) (M_w =2.0 × 10^5 g/mol) and poly (D-lactide) PDLA (M_w =7.0 × 10^4 g/mol) were purchased from Total Corbion PLA BV (Gorinchem, Netherlands). Absolute ethanol, phosphate buffered saline (PBS) were supplied by Sigma-Aldrich Inc, China. New Zealand rabbits were purchased from the laboratory animal center of the Fourth Military Medical University. Live/Dead Baclight Bacterial Viability Kit and fibroblast L929 were purchased from Thermo Fisher Scientific. *S. aureus* (ATCC 29213) and *E. coli* (ATCC 25922) were isolated from Xijing Hospital, China.

Synthesis of 3-(3-(trimethoxysilyl) propyl)-1-vinyl-1H-imidazol-3-ium Chloride (IL) and IL-grafted GO (GO-*g*-IL). IL was synthesized by stirring a mixture containing 3-chloropropyl-trimethoxy silane (0.6 mol/ml) and vinyl imidazole (0.6 mol/ml) at 50 ℃ for 96 hrs. The desired product was separated by ethyl acetate, rotary evaporated and then dried in vacuum drying oven at room temperature for 24 hrs. GO-*g*-IL was then synthesized via dehydration condensation reaction between hydroxy groups on GO and hydrolyzed organosiloxane groups of

3-(3-(trimethoxysilyl)propyl)-1-vinyl-1H-imidazol-3-ium chloride. Typically, GO (0.1 mol) and IL (0.6 mol) were dispersed and dissolved in the mixed solvent (the volume ratio of water/ethyl alcohol was 1:9). The reaction was kept under stirring at a speed of 1100 r/min for 48 hrs. After that, GO-*g*-IL was obtained by centrifugation at 3000 r/min for 5 min. Finally, the product was dissolved in excess ethyl alcohol and filtered via the organic filtering membrane for three times to remove the unreacted IL.

Electrospun Membranes and Trachea Scaffolds Fabrication. PLA, GO or GO-*g*-IL were dissolved into hexafluoroisopropanol. The total concentration of PLA and GO (or GO-*g*-IL) was 10 wt%. The loading level of GO or GO-*g*-IL by weight of PLA was 5%. Stereocomplex PLA (sc-PLA) matrix consisted of equal qualities of PLLA and PDLA. According to the enantiomorph of PLA, stereocomplexation can be formed between PLLA and PDLA. All the PLA matrix used in this work was sc-PLA. Electrospinning flow rate was kept at 0.5 ml/h. The voltage of electric field was applied at 15 kV and collectors positioned 20 cm from the needle tip. There are three kinds of collectors: flat tinfoil, and two grid templates made by copper wires with a unit grid side length of 800 μm and 400 μm, respectively.

Trachea scaffolds were fabricated by integrating 3D printed thermoplastic polyurethane (TPU) skeleton and electrospun membranes. The hollow cylinder skeletons were printed using a 3D Bioprinter (Doworld technology, China), with length and diameter of 5 cm and 0.8 cm, respectively. These skeletons were subsequently wrapped by four-layers of electrospun membranes.

Characterization. The chemical structure of IL was confirmed by proton nuclear magnetic resonance (^{1}H NMR) spectroscopy (400M, Bruker, Germany): ^{1}H NMR (400 MHz, DMSO-d6) δ

8.24 (d, J = 58.9 Hz, 2H), 7.41 (s, 1H), 6.08 (s, 1H), 5.61–5.35 (m, 2H), 4.26 (s, 2H), 3.47 (s, 9H), 1.89 (d, J = 12.2 Hz, 2H), 0.57 (s, 2H).

The Fourier-transform infrared spectroscopy (FT-IR) spectra of pristine vinyl imidazole, 3-chloro propyl-trimethoxy silane and IL were presented and compared in the Supporting Information Figure S1, which were detected by an infrared spectrometer (Bruker, Germany). The characteristic peak at about 736 cm^{-1} of chloride of 3-chloro propyl-trimethoxy silane had disappeared after complete reaction with vinyl imidazole, which could be confirmed by the spectra of IL.

The chemical element characterization of IL and GO-*g*-IL was carried out by X-ray photoelectron spectroscopy (XPS) (Kratos, England); Structural and morphological characterizations of GO and GO-*g*-IL were also investigated by transmission electron microscopy (TEM) (Tecnai G2 F20 S-TWIN, USA) and Raman analysis. Raman measurements were performed by a HR800 LabRam with a laser excitation wavelength of 532 nm at room temperature.

Morphology of Electrospun Membranes. The morphologies of the electrospun fibers and cells on membranes were performed by scanning electron microscopy (SEM) (Vega3, Tescan, Czech Republic).

Mechanical and Hydrophilic Characterization. Mechanical properties of rabbit trachea, electrospinning membranes, and composite scaffolds were evaluated via a universal tensile tester (Instron 5967, USA). Before testing, electrospinning membranes were tailored into 50 × 20 mm rectangle samples with a thickness of 0.05 mm. Test rate was 10 mm/min and at least 5 samples were tested for mechanical properties of each configuration. All the samples were measured by a

micrometer caliper with an average error at 0.01 mm. Young's modulus of the fibrous membranes were measured using a Nanoindenter (Piuma, Netherlands).

The water contact angle measurement was performed by an OCA15EC contact angle device (Beijing North Defei Co. Ltd., Beijing). The water droplet used in the process had a volume of about 4 μL. Final value of the contact angle was an average calculated from 5 data points. Each electrospun membrane sample was measured at 5 different positions.

***In Vitro* Cytocompatibility and Cell Infiltration.** Fibroblasts L929 were incubated on the electrospun membranes to investigate the biocompatibility. Membrane samples were placed into a 6-well plate and seeded with 2 ml cell suspension which containing 1×10^5 L929 cells. After incubating for 36 hrs, samples were removed and placed into a new plate and twice gently rinsed with phosphate-buffered solution. Then cells were settled by 2.5% glutaraldehyde solution at 4 ℃ for 12 hrs. After washing off the fixative by phosphate-buffered saline (PBS) solution, samples were gradually dehydrated by ethanol with a series of concentrations (30, 50, 70, 80, 90, and 100%) for each 15 min. Finally, samples were dried for 12 hrs in a drying oven and coated with platinum for 20 sec prior to SEM examination.

Antibacterial Measurement of Electrospun Membranes. Antibacterial activity against *E. coli* (ATCC 25922) and *S. aureus* (ATCC 29213) of electrospun membranes was investigated. Membrane samples were incubated in bacterial suspension with a cell concentration of 1×10^7 cells/ml for 48 hrs. The surface electrical potential of cells and fibers were detected by an Atomic Force Microscope (AFM) (Dimension, Bruker, Germany). After that, the membranes were rinsed with PBS thrice for removing the dissociative cells. Finally, cells on the electrospun membranes

were fixed after being immersed into 2.5% aqueous glutaraldehyde solution for 1 h and being washed with distilled water. Cells morphologies on membranes were observed by SEM.

Antibacterial quantitative or IC50 (half maximal inhibitory concentration: concentration of composites at which microbial growth was inhibited to 50%) analysis was also performed. During the process, the concentration of bacterial suspensions was 1×10^6 CFU mL^{-1} (Colony-Forming Units). *E. coli* and *S. aureus* were incubated with different concentration sc-PLA, sc-PLA/GO and sc-PLA/GO-*g*-IL composites in test tubes. The concentration of sc-PLA, sc-PLA/GO and sc-PLA/GO-*g*-IL electrospun membranes is 0, 1, 5, 10, 50 and 100 μg/ml, respectively. Incubated tubes were under aerobic conditions at 37 ℃ for different time period. Suspensions absorbance at 600 nm of incubated solutions was detected to estimate bacterial growth.

Dual-mode antibacterial activity assay: Electrospun membranes of sc-PLA/GO and sc-PLA/GO-*g*-IL were incubated in LB medium containing *E. coli* or *S. aureus* 1×10^8 CFU mL^{-1} at 0.05 mM. Using the same mol of sc-PLA membrane as contrast. After cultured for 24 hrs at 37 ℃, the bacteria were collected by centrifugation, and cleaned by PBS for thrice. Then all bacteria were stained by Live/Dead Baclight Bacterial Viability Kit. Confocal laser scanning microscopy (CLSM) (TCS SP8 DIVE, Leica, Germany) was used to investigate the activity of bacteria on the membranes.

***In Vivo* Biocompatibility of Electrospun Membranes and Trachea Scaffolds.** All implantation procedures were approved by animal care committee of the Fourth Military Medical University and in accordance with the National Institute of Health's guide for the care and use of laboratory animals.

In vivo implantation: After immersion in PBS and sterilization by UV light for 24 hrs, the electrospun membranes and trachea scaffolds were implanted into thigh incisions of rabbits. After two- or four-weeks of implantation, new regenerated tissues were harvested and treated by 4% paraformaldehyde for 24 hrs. At the same time, heart, liver, spleen, lung, and kidney tissues of corresponding rabbits were also processed by above-mentioned process. Harvested tissues were embedded in liquid paraffin, and vertically cut into slices with thickness of 3 μm. After that, sliced organs were stained by hematoxylin and eosin (H&E) and Masson trichrome. Finally, they were observed with a Leica SP8 optical microscope.

Hemolysis assay: 3.0 mL fresh blood was provided from a healthy rabbit. Erythrocytes were obtained by process of centrifugation at 1500 rpm for 20 min and flushed with PBS until the supernatant was pellucid. The precipitate Erythrocytes were diluted to 2 vol% by PBS solution. Sterile scaffolds were immersed into the diluted erythrocytes solutions for incubating at 37 ℃ for 3 hrs. Erythrocyte samples incubated with scaffolds matrix were centrifuged by mentioned procedure. After that, supernatant (100 mL) were transferred into a 96-well plate. OD values were detected by an UV-Vis spectrophotometer (DU-800, Beckman, USA) at 576 nm. Erythrocytes treated with water were served as the positive control, while those treated with PBS served as the negative. The concentration of co-incubated matrix was 0.01 mM. The hemolysis rate was calculated by the following formula:

$$\text{Hemolysis rate}\,(\%) = \frac{OD_{sample} - OD_{negative\ control}}{OD_{positive\ control} - OD_{negative\ control}} \times 100\%$$

RESULTS AND DISSCUSSION

Synthesis and Characterization of GO-*g*-IL. GO nanosheets are graphene baseplates covered with several functional groups: hydroxyl, epoxy, carbonyl and carboxyl groups. These oxygen-containing groups, act as trigger points, enabling in-situ reactions on the surfaces of the nanosheets.[36] In this work, GO-*g*-IL nanocomposites were synthesized via two main stages as shown in Scheme 1. First, 3-(3-(trimethoxysilyl)propyl)-1-vinyl-1H-imidazol-3-ium chloride was synthesized by nucleophilic addition reaction between same molar 3-chloro propyl-trimethoxy silane and vinyl imidazole. Second, the terminal alkoxy group of 3-(3-(trimethoxysilyl)propyl)-1-vinyl-1H-imidazol-3-ium chloride was hydrolyzed into hydroxy in water of the mixed solvent (water and alcohol with 5:5 volume ratio). The 3-(3-(trimethoxysilyl)propyl)-1-vinyl-1H-imidazol-3-ium chloride with hydroxy (IL) would occur dehydration and condensation reaction with the hydroxy groups among the surface of GO sheet. The molecular model of GO-*g*-IL is shown in Figure. 1a.

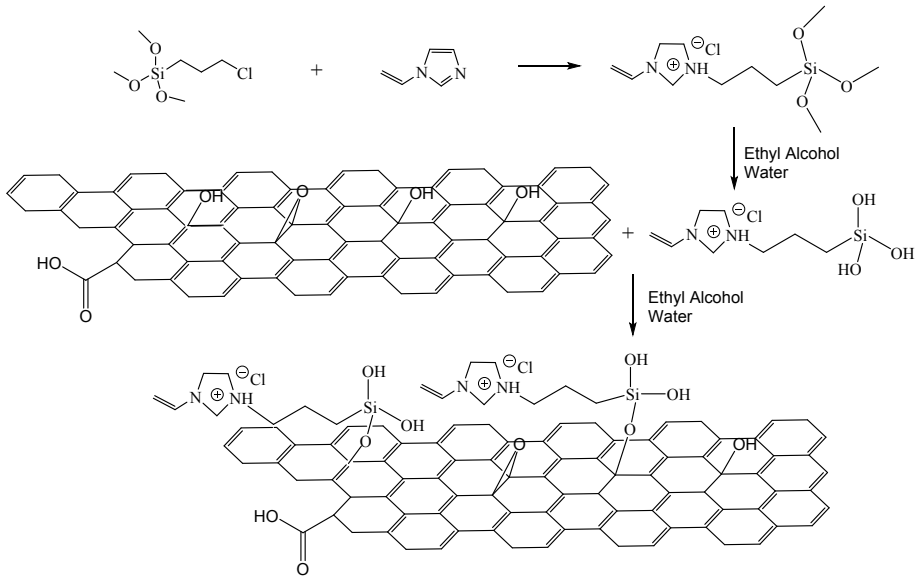

Scheme 1. Diagram of the preparation of the GO-*g*-IL.

Direct morphological evidence of the GO-*g*-IL nanocomposite is given by TEM and Raman spectrum results. Figure. 1c shows the TEM images of GO and GO-*g*-IL. The GO presents a clean surface with a few thin ripples. However, after grafting of IL on the GO surface, there appeared an obvious shadow of deposited IL. Similarly, GO Raman spectra (Figure. 1b) shows the D band, G band and 2D band at 1345, 1604, and 2936 cm^{-1}, respectively. In general, D band refers to a ring breathing mode of sp^2 carbon rings, while the G band relates to the E2g phonon of the sp^2 carbon atom. The D band is more dominant than G band in GO spectra, and reveals that there are abundant defects on the surface of the GO. These defects are caused by acid oxidation during the preparation of GO. The ratio of the D to G band intensities (I_D/I_G) is also related to the degree of disorder in the carbon structure. In the Figure 1b, the ratio of the D to G bands of GO is almost 1.23. However, the ratio of GO-*g*-IL is lower at 1.03. This indicates that the coating of IL grafting on GO has ordered the structure and decreased the number of defects. Furthermore, the intensity ratio of I(G)/I(2D) and G band shifting are used to determine the thickness of layer.[37] A higher ratio or lower wavenumber of the G band refers to an increased layer thickness. In Figure 1b, the intensity ratio of I(G)/I(2D) of GO-*g*-IL is 2.86 which is higher than 2.75 of GO. Also, the wavenumber of the G band decreased from 1615 to1606 cm^{-1} after grafting IL on GO.

To further confirm the chemical structure of GO-*g*-IL, the XPS curves of GO and GO-*g*-IL are recorded in Figure 1d. In the wide spectrum of GO, there are only two peaks that refer to C and O elements. While for GO-*g*-IL, additional peaks of Si, N and Cl appeared, suggesting that IL has been grafted on the surface of GO. The C 1s spectrum of GO (Figure 1d) shows three main peaks at 285 eV, 285.9 eV and 287.8 eV, which could be assigned to the C-C/C-H bond (sp^2), C-O and the existence of O−C=O bonds. For the C 1s spectrum of GO-*g*-IL, the peaks with binding energy at 284.2 and 288.6 are taken for C-Si and C-N bonds, respectively. The additional O-Si

peak at 528.8 eV of O 1s compared to that of GO further illustrates the successful modification of GO.

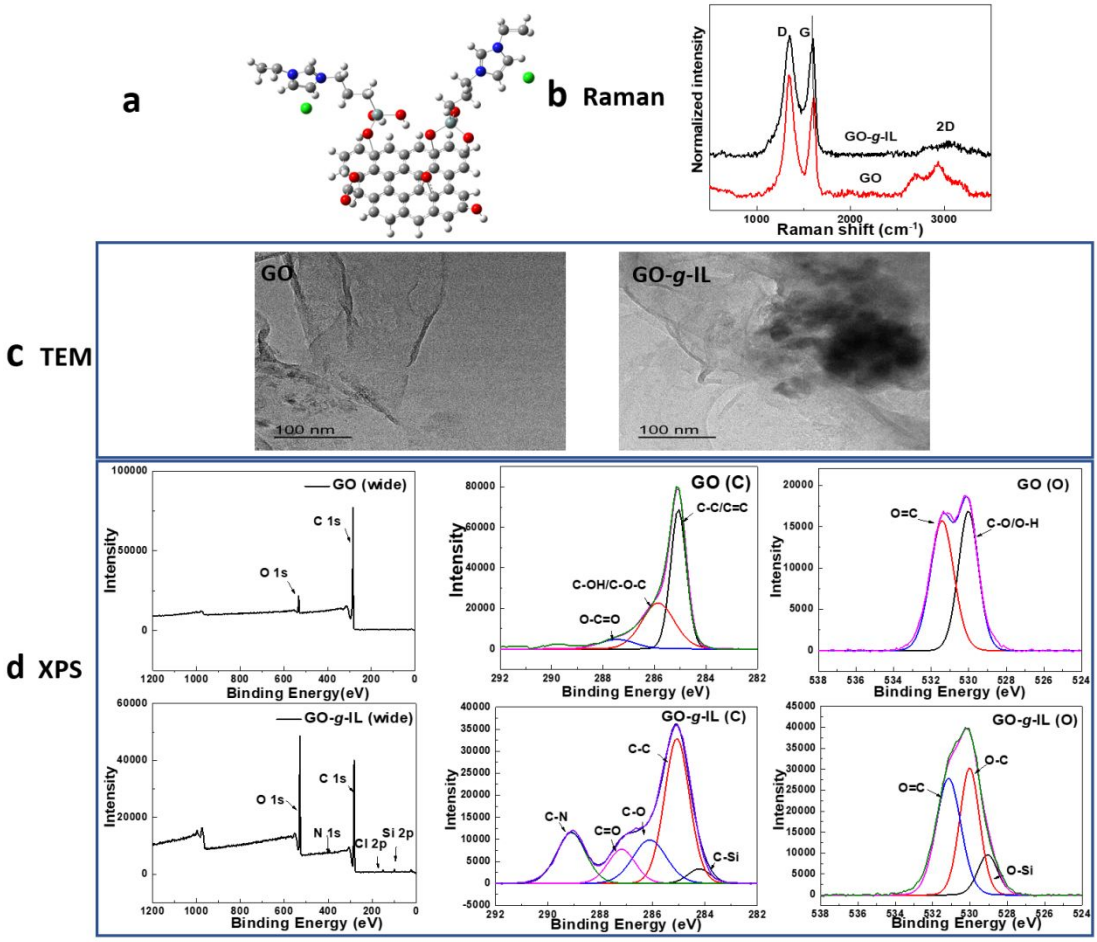

Figure 1. a. Molecular model of GO-*g*-IL; b. Raman curves of GO and GO-*g*-IL; c. TEM graphs of GO and GO-*g*-IL; d. XPS patterns of GO and GO-*g*-IL.

Properties of Electrospun Membranes and Trachea Scaffolds. Electrospinning is commonly considered a simple technique for preparing continuous fibrous network, which can architecturally be similar to the structure of the extracellular matrix (ECM). However, the densely arrangement and inadequate interspace is unable to meet cell penetration, differentiation and further growth inside these electrospun membranes. Here, we sought to use patterned template

electrospinning to induce a regular fibers arrangement. The matrix used for electrospinning is sc-PLA, which has been investigated in our previous work.[12] The effect of stereocomplexation on mechanical property, hydrophilia, and morphology of porous scaffolds, which lead to the conclusion that the stereocomplexation of PLA matrix promoted uniform of microstructures[38]. According to the stereocomplexation effect between PLLA and PDLA, sc-PLA presents stronger thermostability, superior mechanical properties and processing characteristics.[39,40] Therefore, a series of sc-PLA, sc-PLA/GO and sc-PLA/GO-*g*-IL systems for patterned electrospinning was prepared. As the SEM images show in Figure 2a, the electrospun membrane was collected on a conventional tin foil paper. The fibers were distributed randomly with an average diameter distribution of 1.8 ± 0.3μm in Figure 2(a3). For the patterned electrospinning copper grids with 800 μm (Pattern 1) and 400 μm (Pattern 2) side lengths were used as collectors instead of tin foil paper. It was observed that the electrospun products presented a replication of the grid patterns of the collector as shown in Figure 2(b1-2) and 2(c1-2). The walls of these grids, composed of many uniaxially aligned fibers, tend to conglutinate with each other and the cross points apparently become the densest areas. However, as displayed in Figure 2(b3) and (c3), the fibers inside the girds tend to arrange themselves in a loose manner. Due to the low density of the fibers, the pore sizes of Pattern 1 and Pattern 2 in these areas are larger than for the random membranes, as shown in Figure 2(a4), (b4) and (c4). Therefore, the multilevel structure of these fiberous membranes can be tailored by the patterned electrospinning method via controlling the structure of the conductive collector.

As expected, the fibers of patterned electrospun membranes have regularly aligned themselves along the collectors. In order to get more insight into the effect of the patterning structure on the micromechanical properties, Young's modulus measurements were performed by

nanoindentation. For the random membrane, the average value of Young's modulus is 15.6±2.7 kPa (Figure 2a' and 2a"). However, with the grid arrangement of the fibers, the value of Young's modulus of the membranes distributes unevenly. In the case of the Pattern 1 membrane, highly oriented and densely fibrous areas of walls were measured at an average 33.3 ± 3.9 kPa (Figure 2b' and 2b"), which is higher than both the value of 6.6 ± 1.4 kPa inside the grid and for random membranes. Similar results also occur for Pattern 2 with 23.5 ± 3.1 kPa for the walls and 7.0 ± 1.7 kPa inside (Figure 2c' and 2c"). Such significant differences are related to the differences in degrees of compactness of fibers during preparation. It was found that the collector with the larger side length could be used for the preparation of better oriented fibrous structures. Furthermore, the Pattern 1 and Pattern 2 membranes with relative lower stiffness values may offer more favorable conditions for cell infiltration with respect to the central areas of the grids.

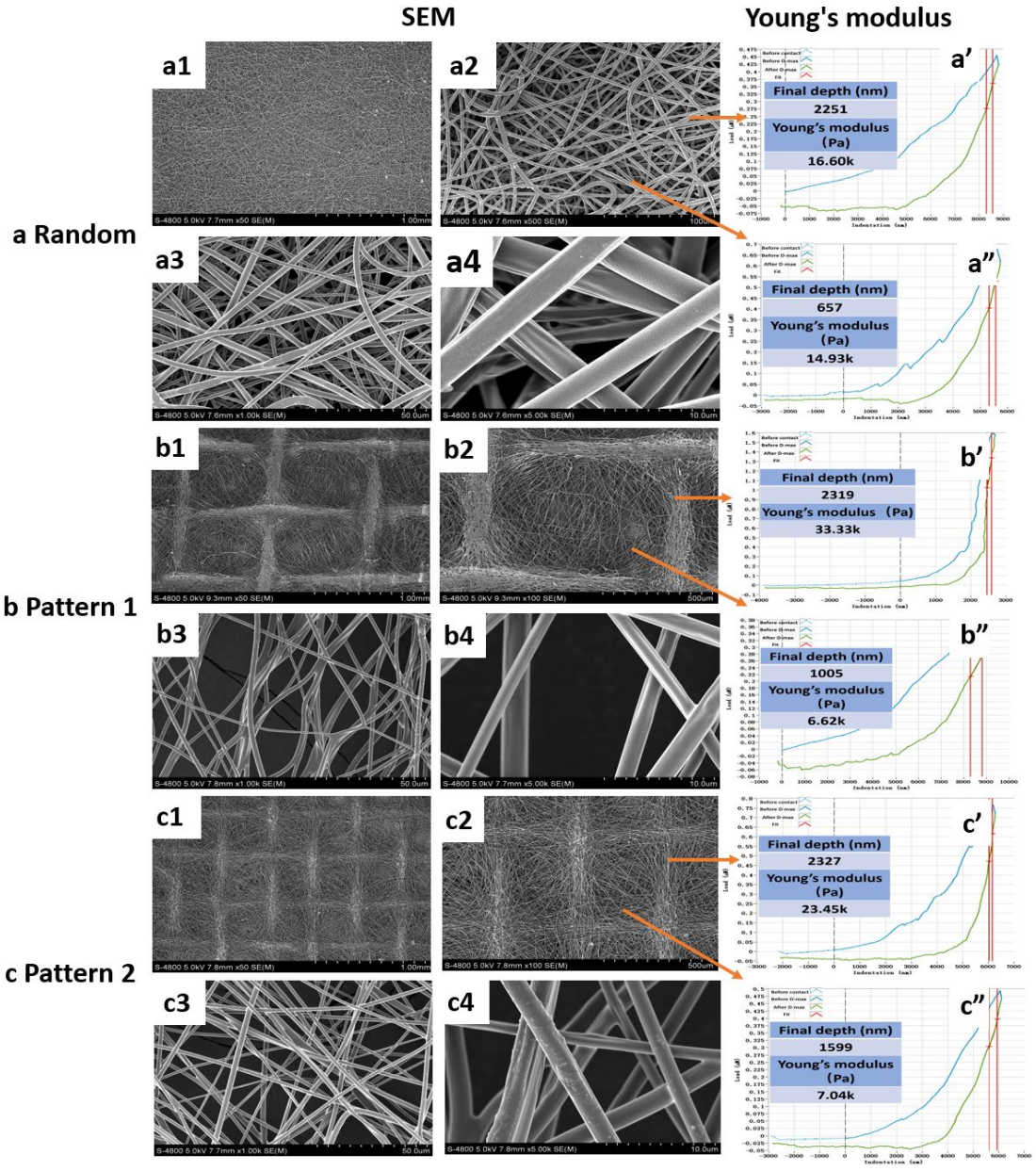

Figure 2. a. Random electrospun membranes: a1-a4. SEM images of random electrospun membranes, a' and a''. Young's modulus of random electrospun membranes; b. Pattern 1 (800 μm) membrane: b1-b4. SEM images, b' and b''. Young's modulus; c. Pattern 2 (400 μm) membrane: c1-c4. SEM images, c' and c''. Young's modulus.

Combined trachea scaffolds in our work were fabricated by combining the 3D-printed TPU skeleton with outer layers of electrospun membranes (Figure 3a). The size of the combined trachea

scaffolds was designed on the basis of the size of actual rabbit trachea taken from the experimental rabbit and literature[34,35]. As the Figure 3a shows, the diameter of the actual rabbit's trachea is about 0.8cm. Therefore, the diameters of combined scaffolds were designed to the same size. The trachea scaffolds *in vivo* will provide supporting strength and prevent collapse of the tracheal lumen during respiratory movements. Here, tensile tests in Figure 3c were performed to evaluate the mechanical properties of electrospun membranes and trachea scaffolds. The sc-PLA membrane in random fiber configuration shows a breaking stress of 4.31 ± 0.67 MPa and an elongation at break of 23.5 ± 3.4%. After the addition of GO and GO-*g*-IL, the breaking stress of the membranes is improved to 5.74 ± 1.1 MPa and 8.41 ± 0.7 MPa, respectively. This may be owing to promoted crystallization of sc-PLA by GO, with GO acting as heterogeneous nuclei.[39] Furthermore, compared to the electrospun membranes with random fiber structure, the patterned membranes exhibit superior properties in terms of both tensile and strain properties. Breaking stress and elongation at break of Pattern 1 sc-PLA/GO-*g*-IL membranes reaches 10.5 ± 2.4 MPa and 49.7 ± 5.2% which is improved by 9.5% and 111% compared to random fiber membranes. Due to the deformation of primary and secondary structures during the tensile testing process, for patterned membranes, the longer side length of the grid structure will lead to more primary deformation. That is also the interpretation for the superior elastic properties of Pattern 1 membranes compared to Pattern 2 as shown in Figure 3c. In terms of breaking stress, the superiority of the patterned electrospun membranes come from its higher degree of orientation of the fibers and cross points of fibers beams. The oriented fibers enhance the breaking stress while the cross points hinder fiber elongation during stretching.

The natural trachea of rabbits possesses the characteristics of soft ductile materials (Figure 3b) and exhibits a high elongation at break of 73 ± 9.1% and a relatively low breaking stress of 9.8 ± 1.9 MPa. However, the single TPU skeleton possesses superior mechanical properties (breaking

stress of 43.7 ± 5.1MPa and an elongation at break of 129 ± 12.1%) Furthermore, the artificial composite trachea made by the TPU skeleton and PLA/GO-*g*-IL electrospun membranes present a higher breaking stress. The breaking stress (with Pattern 1 membrane: 82 ± 6.7 MPa, with Pattern 2 membrane: 85 ± 7.1MPa) of scaffolds composed of patterned membranes are clearly enhanced. These trachea scaffolds exhibit higher strength and a more similar elasticity to native tracheas. In this regard, combined trachea scaffolds would be able to offer appropriate mechanical behavior to prevent the collapse of tracheal lumen in a potential application.

For the electrospun membranes designed for application in tissue engineering, suitable hydrophilic is an indispensable condition for cell attachment, proliferation, and differentiation. The surface of sc-PLA collected on tin foil paper shows a relative high wetting angle of 127.3˚ in the water contact angle test (Figure 3b). While the contact angle is 117.7˚ for membranes with introduced GO nanosheets containing hydrophilic groups including hydroxyl and carboxyl. More significant improvements can be observed after the addition of GO-*g*-IL to the system. Ionic liquid rich in ions will promote the interaction between water and fibers, leading to a lower contact angle value. Furthermore, the pattern grid structure has a positive effect on the hydrophilia of fibrous membranes. The value of contact angle is reduced to 88.4˚ and 54.6˚ with Pattern 1 and Patttern 2 structures, respectively.

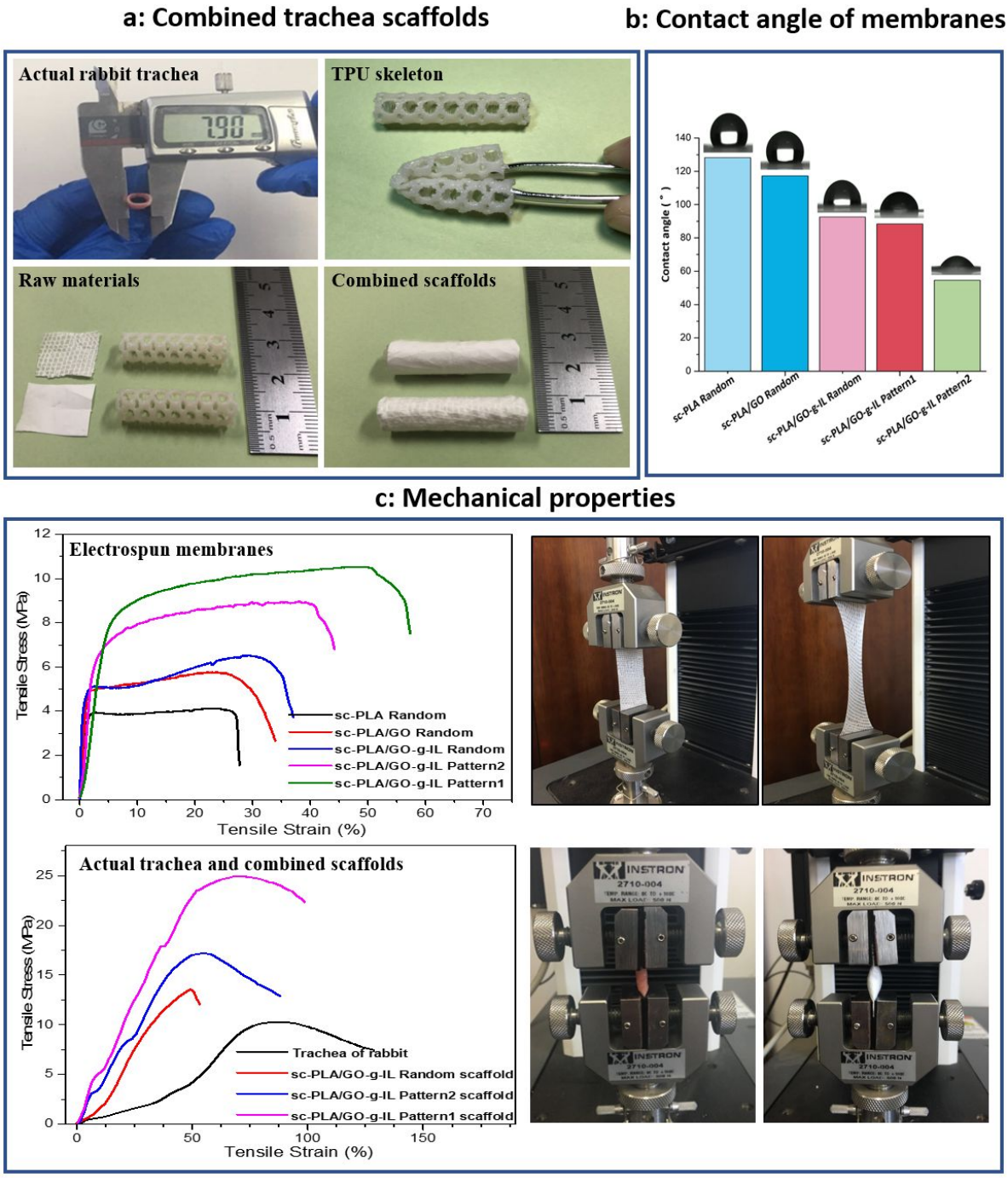

Figure 3. a: Photograph of the actual trachea of rabbit and the raw materials of combined scaffolds; b: contact angle of eletrospun membranes; c: mechanical properties of electrospun membranes and scaffolds.

Antibacterial Activities of Electrospun Membranes. For many tissues, such as, nasal cavity, skin, oral cavity, trachea in human body are contacting directly with air and at risk of bacterial infection. It is essential for the tissue-engineered trachea to possess its own antibacterial ability. GO and GO-*g*-IL were introduced into matrix sc-PLA with the purpose of improving the efficiency of antibacterial. *E. coli* and *S. aureus* were used to investigate the antimicrobial activity of the sc-PLA, sc-PLA/GO and sc-PLA/GO-*g*-IL fibrous membranes. The antibacterial ability of three samples was evaluated by the half maximal inhibitory concentration (IC_{50}) and minimum bactericidal concentration (MBC). Figure 4 shows the OD_{600} value of *E. coli* and *S. aureus* with a series of concentrations of electrospun membranes in nutrient solution after cultured 6 hrs. Here, the bacteria for IC_{50} evaluation were cultured in bacteriological incubator at 37℃. For MBC evaluation, the bacteria were cultured under shaking at same temperature. Compared to the group treated with sc-PLA which showed a relative steady OD_{600} value, the values of groups treated with sc-PLA/GO and sc-PLA/GO-*g*-IL are observed to decrease obviously; especially, sharper decrease is observed for group treated with sc-PLA/GO-*g*-IL. Furthermore, as shown in Fig. 4a and 4c, the IC_{50} values of sc-PLA/GO against *E. coli* and *S. aureus* are 55μg/ml and 48 μg/ml respectively. However, the values of sc-PLA/GO-*g*-IL against *E. coli* and *S. aureus* are respectively reduced to 0.8μg/ml and 0.76 μg/ml, illustrating the antibacterial efficiency was enhanced almost 70 times by grafting IL molecular onto GO nanosheets. As for MBC against *E. coli* and *S. aureus*, sc-PLA/GO sample with the maximum concentration has not made the OD_{600} value below three orders of magnitude of control group. However, the MBC value of sc-PLA/GO-*g*-IL could be work out at 211 and 175 μg/ml respectively. Therefore, it can be concluded that the sc-PLA/GO-*g*-IL membrane has a remarkable antibacterial effect on *E. coli* and *S. aureus* which is also in accordance with SEM results (see Fig. S2 in Supporting Information).

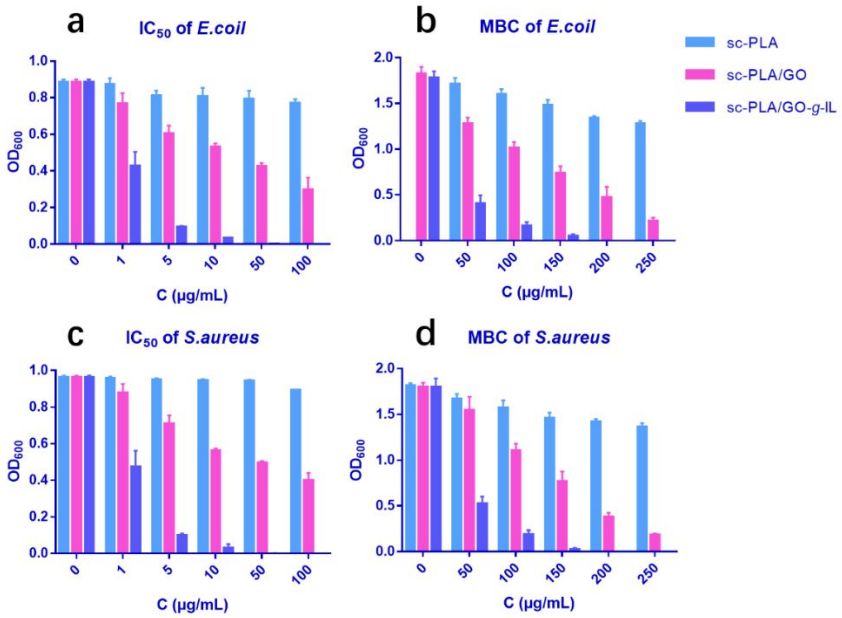

Figure 4. Antibacterial effect of sc-PLA, sc-PLA/GO and sc-PLA/GO-*g*-IL of different concentrations. a: IC50 of *E. coil*; b: MBC of *E. coil*; c: IC50 of *S. aureus*; d: MBC of *S. aureus* (blue column: bacteria treated with sc-PLA; red column: bacteria treated with sc-PLA/GO; purple column: bacteria treated with sc-PLA/GO-*g*-IL)

Due to emerging challenges faced by the bacterial resistance against several drugs, there is a pressing need for the development of new antibiotics with a unique mode of reaction. GO presents special nanostructures with its very sharp edges of nanowalls which can damage the cytomembrane by direct physical contacting.[12] But for reasons that anions such as carboxyl, phosphoryl and glycerate groups in proteins or polysaccharides will be deprotonated to produce negatively charged cytomembrane, the antibacterial mechanism of IL reported is mainly due to electrostatic interactions between cationic lipids and bacterial envelope, which disrupts the bacterial envelope by removing positively charged divalent counterions.[41] In order to further investigate the antibacterial mechanism and efficiency of the electrospun membrane. AFM and CLSM were used to detect the surface potential of *S. aureus* and the contacted fibers and distribution of dead and living bacteria, respectively. From the AFM graphs shown in Figure 5i, *S. aureus* cells are cultured

and attach on the surface of the fibers. The cells on the sc-PLA fibers maintain well-rounded with integrated morphologies. (Figure 5a and a') The surface potentials of cell clusters and the fibers below are measured to be -0.169 V and -0.324 V, respectively. After the addition of GO, the shape of the cells on the sc-PLA/GO fibers has developed into oval or flat morphologies (Figure 5b and b') and the surface potential value is still negative at -0.191 V. Therefore, the added GO has partly destroyed the structure of the cells. However, with the massive positive ions from the introduced GO-*g*-IL, the surface potential value of cells and the sc-PLA/GO-*g*-IL fibers has been inversed into positive values of 0.186 V and 0.297 V. Simultaneously, the cells on the fibers show severe deformations (Figure 5c and c'). There have been similar reports on antibacterial by charge reversal.[42,43]

The CLSM graphs are more intuitively and show the difference in antibacterial effect for the three types of electrospun membranes. As shown in Figure 5, the green semaphores stand for living cells while the red semaphores are for dead cells. The arrangement of fibers in either random or Pattern 2 membranes can be easily observed, simply because the cells were absorbed onto the surface of the fibers by electrostatic interaction. Most of cells on sc-PLA fibers develop into green, illustrating that they are not under threat (Figure 5d and d'). However, there emerges lots of red semaphores on the sc-PLA/GO fibers which mean the added GO has killed part of the cells (Figure 5e and e'). Finally, the fibers of sc-PLA/GO-*g*-IL present the strongest antimicrobial activity on which the cells are mostly destroyed as revealed by the massive red signals in the Figure 5f and f'. A similar conclusion can be drawn from the SEM images shown in Figure S2. The amount of cells on the fibers decreased obviously with GO and GO-*g*-IL doped into the PLA matrix. We also observed that the cytomembranes are broken and even fractured, especially in the case of sc-

PLA/GO-*g*-IL fibers as shown in Figure S2d1 and d2. This also illustrates that there has been a strong interaction between cells and cationic groups of IL.

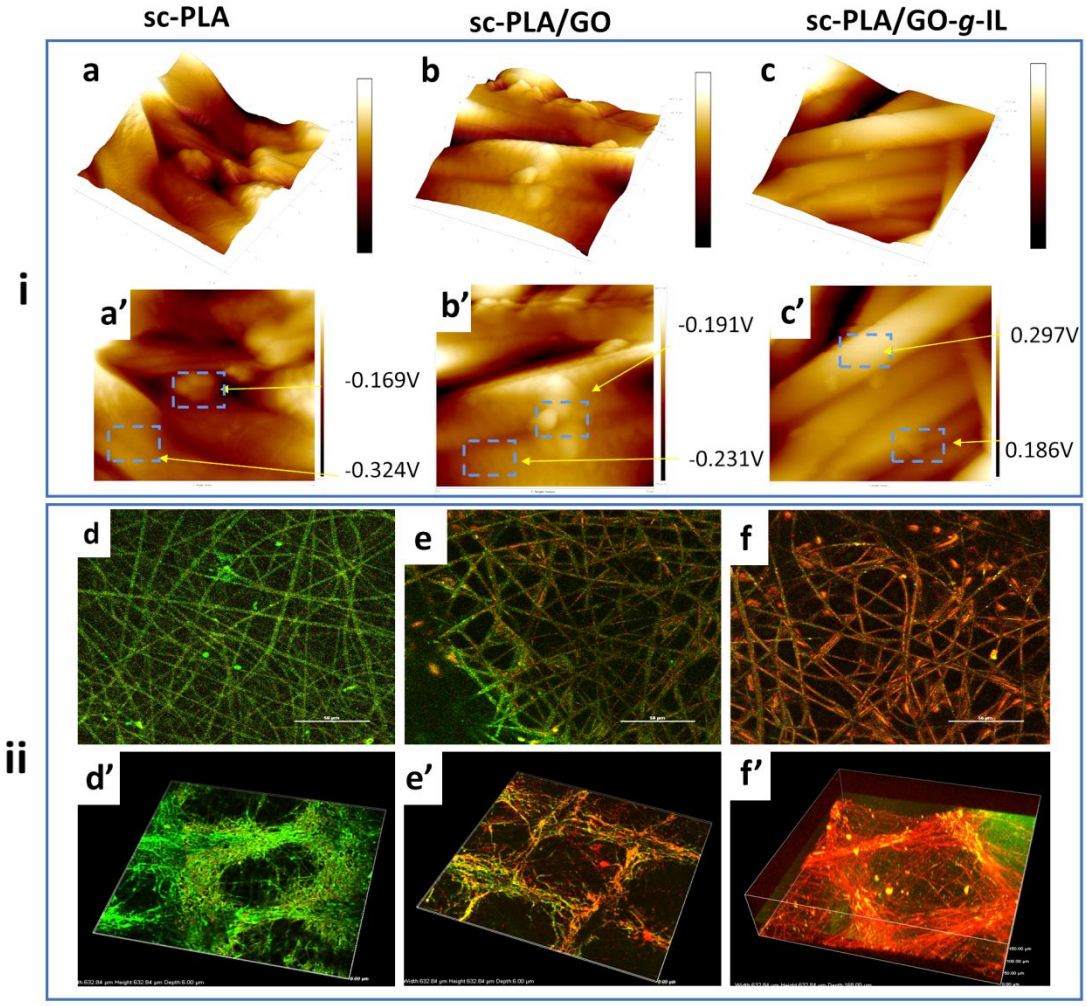

Figure 5. ⅰ: The changes in the surface potential of *S. aureus* cultured on electrospun membranes and fibers: a) the 3D morphology of *S. aureus* cultured on sc-PLA membrane; a') the surface potential of *S. aureus* and sc-PLA fibers; b) morphology of *S. aureus* cultured on sc-PLA/GO membrane; b') the surface potential of *S. aureus* and sc-PLA/GO fibers; c) morphology of *S. aureus* cultured on sc-PLA/GO-*g*-IL membrane; c') the surface potential of *S. aureus* and sc-PLA/GO-*g*-IL fibers.

ⅱ: CLSM graphs of colored *S. aureus* on electrospun membrane: d) *S. aureus* on sc-PLA random membrane; d') *S. aureus* on sc-PLA Pattern 2 membrane; e) *S. aureus* on sc-PLA/GO random membrane; e') *S.*

aureus on sc-PLA/GO Pattern 2 membrane; f) *S. aureus* on sc-PLA/GO-*g*-IL random membrane; f') *S. aureus* on sc-PLA/GO-*g*-IL Pattern 2 membrane.

The Property of Promoting Infiltration of Seed Cells. Before tissue engineered scaffolds will be transplanted to replace problematic organs in the human body, it is necessary to possess a three-dimensional (3D) architecture for cell attachment, growth, and migration. Previous studies on fibrous membranes have shown that despite cells can show favorable cellular adhesion to fibers, it is rare to find cells to infiltrate deep into electropsun fiber mats.[44-47] As shown for the case of random electrospun membranes in Figure 6a, the cells adhered and grew uniformly on the surface of membrane collected on traditional flat tinfoil. Here, the small interspaces formed by dense and randomly oriented fibers does not benefit cell infiltration and a 3D cell arrangement. However, compared to random fibrous membranes, the patterned structure of Pattern 1 and Pattern 2 membranes is able to induce cell growth into the internal space of the fiber membranes. As can be viewed Pattern 1 and Pattern 2 membranes in Figure 6c1 and b1, a good deal of cells attached on quadrilateral with few can be found on the edges. Furthermore, in the magnified images shown in Figure 6b2-3 and c2-3, it can be seen that cells adhered not only to the surface of the membranes but also infiltrated inside the loose fibrous network. Cells were observed fully flattened, expanded in a normal phenotypic shape, and well attached to the fibers under the surface (Figure 6b4 and c4). This evidence illustrates that patterned structures of fibrous membranes positively imitated ECM to provide a penetrable 3D fibrous environment for cells to adhere, infiltrate, and proliferate.

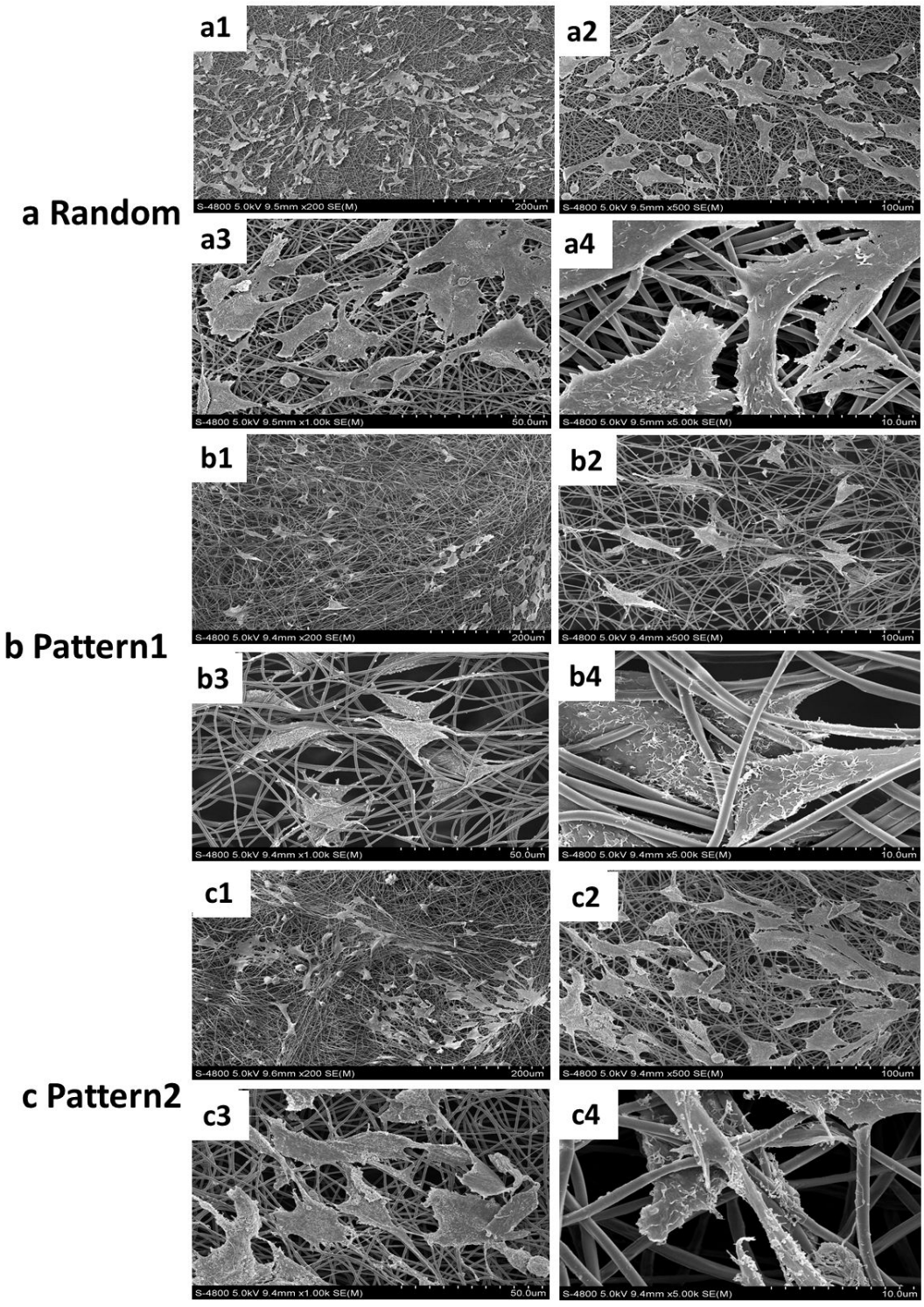

Figure 6. The SEM images of L929 cells incubated on electrospun membranes with 200, 500,1000 and 5000 amplification: a. Random fibrous membrane; b. Pattern 1 membrane; c. Pattern 2 membrane

***In Vivo* Biocompatibility of Electrospun Membranes and Trachea Scaffolds**. A suitable synthetical design of scaffolds is essential for better tissue regeneration *in vivo*. Various chemical and physical cues including types of matrix, growth factors, and structures have been reported to promote tissue regeneration.[48,49] In literature[33-35, 50], embedding artificial scaffolds subcutaneous or in the muscle is a common method. Therefore, in this work, the electrospinning membranes and combined scaffolds were implanted subcutaneous and into the rabbit's thigh respectively. For further evaluating the effects of patterned structures of electrospun membrane cues on tissue regeneration *in vivo*, the layered electrospun membranes with random and Pattern 1 structure were implanted subcutaneously in rabbits. The H&E histology analysis of tissue sections of implanted membranes are shown in Figure 7i. Neither visible inflammation nor infection is observed on the harvested specimens. Moreover, there is no obvious interfacial transition zone between the layered electrospun membranes and subcutaneous tissues (Figure 7i), suggesting that the membranes possess favorable biocompatibility. Interestingly, significantly enhanced regenerative cell attachement appeared on the fibers for the Pattern 1 membranes at 2 weeks after implantation compared to that on random fiber membranes (Figure 7a and 7b). This improved proliferation *in vivo* is likely due to better cell infiltration and tissue ingrowth capacity of the Pattern 1 membranes as discussed above for the *in vitro* experiments. Therefore, both *in vitro* and *in vivo* results indicated that cell differentiation and multiplication inside the Pattern 1 membrane is greatly promoted by the patterned structures. Furthermore, from the H&E staining images of random and Pattern 1 electrospun membranes at 4 weeks shown in Figure 7c and 7d, the fiber membranes have developed some degree of degradation. Interestingly, the degradation of the Pattern 1 layered membranes is more apparent. Most parts of the fiber membranes have fractured and even the fibers themselves are gradually disappearing. The causes of accelerated degradation for this type of

membrane may be related to the enhanced cell activity on the fibers of patterned membranes. The result *in vivo* confirms the superiority of patterned fibrous membranes with respect to cell infiltration, which is consistent with the SEM *in vitro* observations.

In order to further investigate the biocompatibility of the combined trachea scaffolds, the trachea scaffolds composed of sc-PLA and sc-PLA/GO-*g*-IL electrospun membranes were implanted into the muscular tissues of rabbits for 4 weeks. The H&E and Masson histology photographs of cross-cutting implanted scaffolds are shown in Figure 7 ii . There is no obvious inflammation or infection observed on the regenerative tissues or around the scaffolds, illustrating the viable biocompatibility of the trachea scaffolds. As shown in Figure 7e and 7g, the sc-PLA electrospun membranes between the 3D-printed PLA skeleton and regenerative intramuscular tissues can be seen to tightly follow the contours of the skeleton. Besides, regenerative intramuscular tissues have emerged between the interlaminar space of the layered sc-PLA electrospun membranes (Yellow arrows). However, as shown in Figure 7f and 7h, there is no obvious demarcation line between the electrospun membranes and regenerative tissues in the combined trachea scaffolds with sc-PLA/GO-*g*-IL electrospun membranes (Yellow arrows). This superior compatibility may be attributed to a large number of ion activity of the sc-PLA/GO-*g*-IL electrospun fibers.

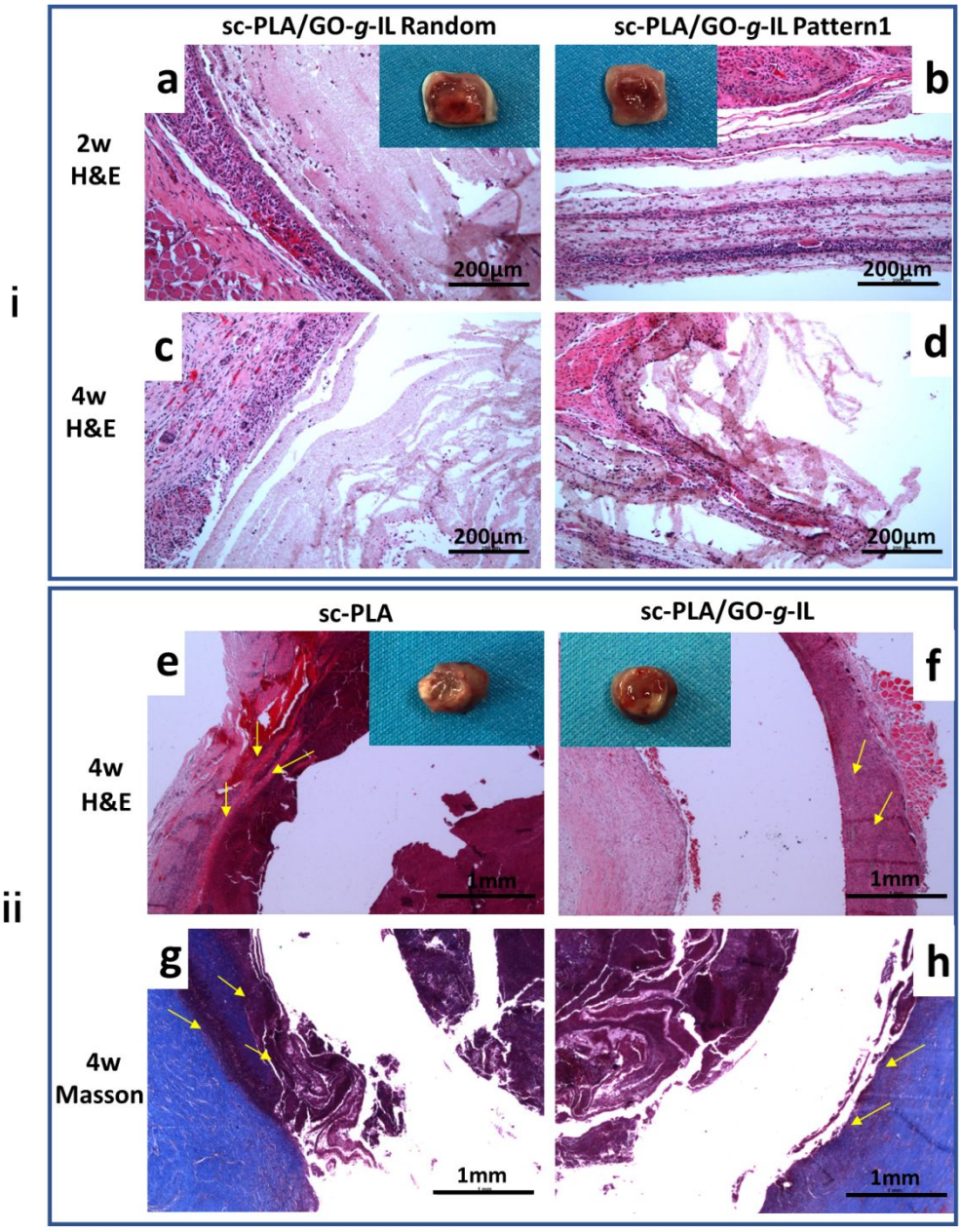

Figure 7. i H&E staining photography of sections of electrospun membranes: a. random sc-PLA/GO-*g*-IL membrane at 2 weeks after implantation *in vivo*; b. Pattern 1 sc-PLA/GO-*g*-IL membrane at 2 weeks; c. random sc-PLA/GO-*g*-IL membrane at 4 weeks; d. Pattern 1 sc-PLA/GO-*g*-IL membrane at 2 weeks.

ii H&E staining photography of sections of trachea scaffolds: Trachea scaffold composed of sc-PLA (e) and sc-PLA/GO-*g*-IL (f) electrospun membrane at 4 weeks after implantation *in vivo*; Masson trichrome staining

photography of sections of trachea scaffolds: Trachea scaffold composed of sc-PLA (g) and sc-PLA/GO-*g*-IL (h) electrospun membrane at 4 weeks after implantation *in vivo*.

As the trachea scaffolds will be in direct contact with tissues and blood in practical clinical applications, it is necessary to evaluate their hemocompatibility and cytotoxicity. Compared to the broken-up shape of erythrocyte in water, the morphologies of erythrocyte in sc-PLA, sc-PLA/GO and sc-PLA/GO-*g*-IL samples can be seen fully intact in Figure 8D. This illustrates that the materials of trachea scaffolds have no obviously hemolysis effect on the red blood cells. The hemolysis rates of the corresponding samples are shown in Figure 8E. All the values of the three materials present in the trachea scaffolds are below 5%. This also illustrates that there is no obvious hemolysis effect and that the material system shows a good compatibility with blood. Furthermore, to evaluate the biosafety of the scaffolds *in vivo*, the main tissues of the implanted rabbit including heart, liver, spleen, lung, and kidney were harvested for H&E staining (Figure 8A). There are no abnormal damages or effects observed, which indicates that these fibrous membranes and trachea scaffolds are potential safe materials for clinical applications.

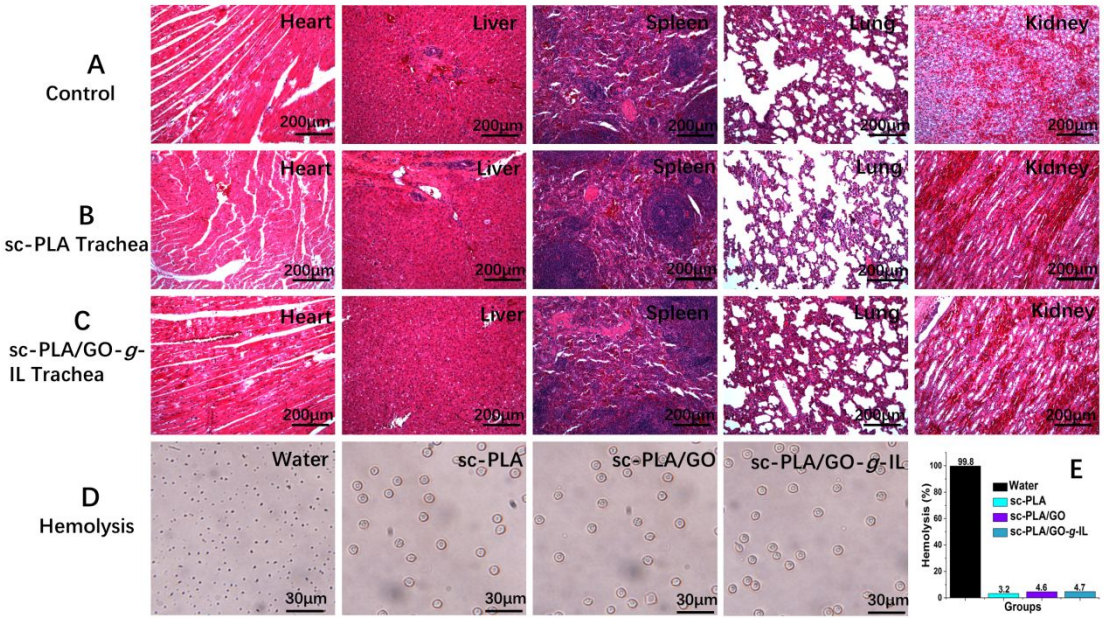

Figure 8. A: H&E staining of the heart, liver, spleen, lung, and kidney tissues harvested from the control rabbit; B and C: H&E staining of the tissues of rabbits after 28 days treatment by sc-PLA trachea and sc-PLA/GO-*g*-IL trachea scaffold, respectively; D: micrographs of red blood cells treated by different materials preparing for trachea scaffolds; E: hemolysis rate for the groups with different treatment.

CONCLUSION

In summary, trachea scaffolds were developed by combining antibacterial patterned electrospun membranes with 3D-printed skeletons. Compared to random fibrous membranes, the patterned membranes were able to substantially improve the mechanical property and hydrophilia. Additionally, *in vitro* results demonstrated that the patterned fibrous membranes promoted tissue regeneration. Furthermore, the sc-PLA/GO and sc-PLA/GO-*g*-IL membranes were investigated against *E. coli* and *S. aureus* cells, showing excellent antibacterial effects. Moreover, the *in vivo* results indicated that patterned fibrous membranes and trachea scaffolds possessed favorable biocompatibility and facilitated considerable new tissue formation in a rabbit model. Therefore, both *in vitro* and *in vivo* results indicated that combined trachea scaffolds would be desired for tracheal repair or transplant applications.

ASSOCIATED CONTENT

Supporting information

The Supporting Information is available free of charge on the ACS Publications website.

Characterization of pristine vinyl imidazole, 3-chloro propyl-trimethoxy silane and IL

SEM images of S. aureus and E. coli incubated on different electrospun membranes.

AUTHOR INFORMATION

Corresponding Authors

*E-mail: shixuetao@nwpu.edu.cn

*E-mail: zhangguc@nwpu.edu.cn

ORCID

Yuan Kang: 0000-0002-1720-3002

Notes:

The authors declare no competing financial interest.

Those authors Yuan Kang, Chaoli Wang and Youbei Qiao contributed equally to this study.

ACKNOWLEDGMENT

This work is funded by the National Natural Science Foundation of China (No. 51773170) and the Fundamental Research Funds for the Central Universities (Grant No. 3102018jcc006). We would like to thank the Analytical & Testing Center of Northwestern Polytechnical University for equipment supporting.

REFERENCES

(1) Baiguera, S.; Jungebluth, P.; Burns, A.; Mavilia, C.; Haag, J.; Coppi, P. D.; Macchiarini P. Tissue engineered human tracheas for *in vivo* implantation. *Biomaterials* **2010**, *31*, 8931-8938.

(2) Agarwal, S.; Wendorff, J.H.; Greiner, A. Progress in the field of electrospinning for tissue engineering applications. *Adv. Mater.* **2009**, *21*, 3343-3351.

(3) Townsend, J.M.; Ott, L. M.; Salash, J.R.; Fung, K.; Easley, J.T.; Seim III, H.B.; Johnson, J.K.; Weatherly, R.A.; Detamore, M.S. Reinforced electrospun polycaprolactone nanofibers for tracheal repair in an *in vivo* ovine model. *Tissue. Eng. Part A.* **2018**, *24*, 1301-1308.

(4) Kobayashi, K.; Suzuki, T.; Nomoto, Y.; Tada, Y.; Miyake, M.; Hazama, A.; Wada, I.; Nakamura, T.; Omori, K. A tissue-engineered trachea derived from a framed collagen scaffold, gingival fibroblasts and adipose-derived stem cells. *Biomaterials* **2010**, *31*, 4855-4863.

(5) Peijs, T. Electrospun polymer nanofibers and their composites. In Comprehensive Composite

Materials II; Elsevier: New York, NY, USA, 2018; Volume 6, pp. 162–200.

(6) Azeem, A.; Marani, L.; Fuller, K.; Spanoudes, K.; Pandit, A.; Zeugolis, D. I. Influence of Nonsulfated Polysaccharides on the Properties of Electrospun Poly(lactic-co-glycolic acid) Fibers. *ACS Biomater. Sci. Eng.* **2017**, *3*, 1304-1312.

(7) Zhang, C.; Wang, L.; Zhai, T.; Wang, X.; Dan, Y.; Turng, L. S. The surface grafting of graphene oxide with poly(ethylene glycol) as a reinforcement for poly(lactic acid) nanocomposite scaffolds for potential tissue engineering applications. *J. Mech. Behav. Biomed*. **2016**, *53*, 403-413.

(8) Visscher, L. E.; Dang, H. P.; Knackstedt, M. A.; Hutmacher, D. W.; Tran, P. A. 3D printed polycaprolactone scaffolds with dual macro-microporosity for applications in local delivery of antibiotics. *Mat. Sci. Eng. C-Mater.* **2018**, *87*, 78-89.

(9) Mandal, B. B.; Park, S. H.; Gil, E. S.; Kaplan, D. L. Multilayered silk scaffolds for meniscus tissue engineering. *Biomaterials*, **2011**, *32*, 639-651.

(10) Hughes-Brittain, N.F.; Qiu, L.; Picot, O.T.; Wang, W.; Peijs, T.; Bastiaansen, C.W. Surface texturing of electrospun fibres by photoembossing using pulsed laser interference holography and its effects on endothelial cell adhesion. *Polymer* **2017**, *125*, 40-49.

(11) Qiu, L.; Hughes-Brittain, N.F.; Bastiaansen, C.W.; Peijs, T.;Wang, W. Responses of vascular endothelial cells to photoembossed topographies on poly(methyl methacrylate) films. *J. Funct. Biomater.* **2016**, 7, 33.

(12) Chen, H.; Malheiro, A.; Van, C. B.; Mota, C.; Wieringa, P. A.; Moroni, L. Direct writing electrospinning of scaffolds with multi-dimensional fiber architecture for hierarchical tissue engineering. *ACS Appl. Mater. Interfaces.* **2017**, *9*, 38187-38200.

(13) He, X. X.; Zheng, J.; Yu, G. F.; You, M. H.; Yu, M.; Ning, X.; Long Y. Z. Near-field

electrospinning: progress and applications. *J. Phys. Chem. C* **2017**, *121*, 8663-8678.

(14) Zhang, D.; Chang, J. Electrospinning of three-dimensional nanofibrous tubes with controllable architectures. *Nano Lett.* **2012**, *10*, 3283-3287.

(15) Zhang, D.; Chang, J. Patterning of electrospun fibers using electroconductive templates. Adv. Mater. **2010**, *19*, 3664-3667.

(16) Kang, Y.; Wang, C.; Shi, X.; Zhang, G.; Chen, P.; Wang, J. Crystallization, rheology behavior, and antibacterial application of graphene oxide- graft -poly (l-lactide)/poly (l-lactide) nanocomposites. *Appl. Surf. Sci.* **2018**, *451*, 315-324.

(17) Huangfu, Y.; Liang, C.; Han, Y.; Qiu, H.; Song, P.; Wang, L.; Kong, J.; Gu, J. Fabrication and investigation on the Fe_3O_4/thermally annealed graphene aerogel/epoxy electromagnetic interference shielding nanocomposites. *Compos. Sci. Technol.*, **2019**, 169, 70-75.

(18) Luo, C.; Jiao, T.; Gu, J.; Tang Y.; Kong, J. Graphene Shieled by SiBCN Ceramic: A Promising High Temperature Electromagnetic Wave-Absorbing Material with Oxidation Resistance, *ACS Appl. Mater. Interfaces*, **2018**, 10, 39307-39318.

(19) Liu, S.; Zeng, T. H.; Hofmann, M.; Burcombe, E.; Wei, J.; Jiang, R.; Kong, J.; Chen, Y. Antibacterial activity of graphite, graphite oxide, graphene oxide, and reduced graphene oxide: membrane and oxidative stress. *ACS Nano* **2011**, *5*, 6971-6980.

(20) Kim, T. I.; Kwon, B.; Yoon, J.; Park, I. J.; Bang, G. S.; Park, Y.; Seo, Y. S.; Choi S. Y. Antibacterial activities of graphene oxide-molybdenum disulfide nanocomposite films. *ACS Appl. Mater. Interfaces* **2017**, *9*, 7908-7917.

(21) Zou, F.; Zhou, H.; Jeong, D. Y.; Kwon, J.; Eom, S. U.; Park, T. J.; Hong, S. W.; Lee, J. Wrinkled surface-mediated antibacterial activity of graphene oxide nanosheets. *ACS Appl. Mater. Interfaces* **2017**, *9*, 1343−1351.

(22) Hu, W.; Peng, C.; Luo, W.; Lv, M.; Li, X.; Li, D.; Huang, Q.; Fan, C. Graphene-based antibacterial paper. *ACS Nano* **2010**, *4*, 4317-4323.

(23) Cai, X.; Tan, S.; Lin, M.; Xie, A.; Mai, W.; Zhang, X.; Lin, Z.; Wu, T.; Liu, Y. Synergistic antibacterial brilliant blue/reduced graphene oxide/quaternary phosphonium salt composite with excellent water solubility and specific targeting capability. *Langmuir* **2011**, *27*, 7828–7835.

(24) Jovanović, S.; Holclajtner-Antunović, I.; Uskoković-Marković, S.; Bajuk-Bogdanović, D.; Pavlović, V.; Tošić, D.; Milenković, M.; Marković, B. T. Modification of graphene oxide surfaces with 12-molybdophosphoric acid: structural and antibacterial study. *Mater. Chem. Phys.* **2018**, *213*, 157-167.

(25) Shuai, C.; Guo, W.; Wu, P.; Yang, W.; Hu, S.; Xia, Y., Feng, P. A graphene oxide-Ag co-dispersing nanosystem: dual synergistic effects on antibacterial activities and mechanical properties of polymer scaffolds. *Chem. Eng. J.* **2018**, *347*, 322-333.

(26) Zhong, L.; Liu, H.; Samal, M.; Yun, K. Synthesis of ZnO nanoparticles-decorated spindle-shaped graphene oxide for application in synergistic antibacterial activity. *J. Photoch. Photobio. B* **2018**, *183*, 293-301.

(27) Fathalipour, S.; Mardi, M. Synthesis of silane ligand-modified graphene oxide and antibacterial activity of modified graphene-silver nanocomposite. *Mat. Sci. Eng. C-Mater*, **2017**, *79*, 55-65.

(28) Zheng, Z.; Xu, Q.; Guo, J.; Qin, J.; Mao, H.; Wang, B.; Yan, F. Structure–antibacterial activity relationships of imidazolium-type ionic liquid monomers, poly(ionic liquids) and poly(ionic liquid) membranes: effect of alkyl chain length and cations. *ACS Appl. Mater. Interfaces* **2016**, *8*, 12684-12692.

(29) Wang, Y. W.; Cao, A.; Yu, J.; Xin, Z.; Liu, J. H.; Liu, Y.; Wang, H. Superior antibacterial activity of zinc oxide/graphene oxide composites originating from high zinc concentration localized around bacteria. *ACS Appl. Mater. Interfaces* **2014**, *6*, 2791-2798.

(30) Zheng, Z.; Guo, J.; Mao, H.; Xu, Q.; Qin, J.; Yan, F. Metal-containing poly(ionic liquid) membranes for antibacterial applications. *ACS Biomater. Sci. Eng.* **2017**, *3*, 922-928.

(31) Qin, J.; Guo, J.; Xu, Q.; Zheng, Z.; Mao, H.; Yan, F. Synthesis of pyrrolidinium-type poly(ionic liquid) membranes for antibacterial applications. *Acs Appl. Mater. Interfaces* **2017**, *9*, 10504-10511.

(32) Law, J.X.; Liau, L.L.; Aminuddin, B.S.; Ruszymah, B.H. I. Tissue-engineered trachea: A review. *Int. J. Pediatr. Otorhinolaryngol.* **2016**, *91*, 55-63.

(33) Park, J. H.; Hong, J. M.; Ju, Y. M.; Jin, W. J.; Kang, H. W.; Sang, J. L.; Kim, S. W.; Kim, S. H.; Cho, D. A novel tissue-engineered trachea with a mechanical behavior similar to native trachea. *Biomaterials* **2015**, *62*, 106-115.

(34) Hsieh, C.; Liao, C.; Dai, N.; Tseng, C.; Yen, B.L.; Hsu, S. 3D printing of tubular scaffolds with elasticity and complex structure frommultiple waterborne polyurethanes for tracheal tissue engineering. *Appl. Mater. Today* **2018**, *12*, 330-341.

(35) Xu, Y.; Li, D.; Yin, Z.; He, A.; Lin, M.; Jiang, G.; Song, X.; Hu, X.; Liu, Y.; Wang, J.; Wang, X.; Duan, L.; Zhou, G. Tissue-engineered trachea regeneration using decellularized trachea matrix treated with laser micropore technique. *Acta Biomaterialia* **2017**, *58*, 113-121.

(36) Galpaya, D. Synthesis, characterization and applications of graphene oxide-polymer nanocomposites. *Nature*, **2015**, *448*, 457-460.

(37) Chartarrayawadee, W.; Molloy, R.; Ratchawet, A.; Janmee, N.; Butsamran, M.; Panpai, K. Fabrication of poly(lactic acid)/graphene oxide/stearic acid composites with improved tensile

strength. *Polym. Composite.* **2015**, *38*, 1-11.

(38) Kang, Y.; Chen, P.; Shi, X.; Zhang, G.; Wang, C. Multilevel structural stereocomplex PLA/collagen membranes by pattern electrospinning for tissue engineering. *Polymer* **2018**, *156*, 250–260.

(39) Tsuji, H.; Takai, H.; Saha, S. K. Isothermal and non-isothermal crystallization behavior of poly(L-lactic acid): effects of stereocomplex as nucleating agent. *Polymer* **2006**, *47*, 3826-3837.

(40) Tsuji, H. Poly(lactide) stereocomplexes: formation, structure, properties, degradation, and applications. *Macromol. Biosci.* **2010**, *7*, 1299-1299.

(41) Chen, Z.; Wang, Z.; Ren, J. Enzyme mimicry for combating bacteria and biofilms. *Acc. Chem. Res.* **2018**, *51*, 789−799.

(42) Goel, K.; Bera, S.; Man, S.; Mondal, D. Synthesis of dual functional pyrimidinium ionic liquids as reaction media and antimicrobial agents. *RSC Adv.* **2016**, *6*, 106806-106820.

(43) Li, Q.; Yong, C.; Cao, W.; Wang, X.; Wang, L.; Zhou, J. Xing, X. Fabrication of charge reversible graphene oxide-based nanocomposite with multiple antibacterial modes and magnetic recyclability. *J. Colloid Interf. Sci.* **2018**, *511*, 285-295.

(44) Rosenfeld, Y.; Lev, N.; Shai, Y. Effect of the hydrophobicity to net positive charge ratio on antibacterial and anti-endotoxin activities of structurally similar antimicrobial peptides. *Biochemistry* **2010**, *49*, 853-861.

(45) Babitha, S.; Rachita, L.; Karthikeyan, K.; Shoba, E.; Janani, I.; Poornima, B.; Sai, K. P. Electrospun protein nanofibers in healthcare: a review. *Int. J. Pharm.* **2017**, *523*, 52-90.

(46) Badami, A. S.; Kreke, M. R.; Thompson, M. S.; Riffle, J. S.; Goldstein, A. S. Effect of fiber diameter on spreading, proliferation, and differentiation of osteoblastic cells on

electrospun poly(lactic acid) substrates. *Biomaterials* **2006**, *27*, 596-606.

(47) Chew, S. Y.; Mi, R.; Hoke, A.; Leong, K. W. The effect of the alignment of electrospun fibrous scaffolds on schwann cell maturation. *Biomaterials* **2008**, *29*, 653-661.

(48) Kang, H.; Zeng, Y.; Varghese, S. Functionally graded multilayer scaffolds for *in vivo* osteochondral tissue engineering. *Acta Biomater.* **2018**, *78*, 365-377.

(49) Bittner, S. M.; Guo, J. L.; Melchiorri, A.; Mikos, A. G. Three-dimensional printing of multilayered tissue engineering scaffolds. *Mater. Today* **2018**, *21*, 861-874.

(50) Chen, Z.; Zhong, N.; Wen, J.; Jia, M.; Guo, Y.; Shao, Z.; Zhao X. Porous Three-Dimensional Silk Fibroin Scaffolds for Tracheal Epithelial Regeneration in Vitro and in Vivo. *ACS Biomater. Sci. Eng.* **2018**, *4*, 2977-2985.

Table of Contents